IEEE Access
Multidisciplinary | Rapid Review | Open Access Journal

Received 7 September 2023, accepted 4 November 2023, date of publication 13 November 2023,
date of current version 17 November 2023.

Digital Object Identifier 10.1109/ACCESS.2023.3332120

RESEARCH ARTICLE

Wideband RCS Reduction of a Linear Patch Antenna Array Using AMC Metasurface for Stealth Applications

BAISAKHI BANDYOPADHYAY, (Graduate Student Member, IEEE),
SUDEB BHATTACHARYA, (Graduate Student Member, IEEE),
RAHUL KUMAR JAISWAL, (Graduate Student Member, IEEE),
MONDEEP SAIKIA, (Member, IEEE),
AND KUMAR VAIBHAV SRIVASTAVA, (Senior Member, IEEE)
Indian Institute of Technology Kanpur, Kanpur 208016, India

Corresponding author: Baisakhi Bandyopadhyay (tania.banerjee678@gmail.com)

ABSTRACT This article presents a linear microstrip patch antenna array at the X-band that incorporates an aperiodic artificial magnetic conductor (AMC) metasurface which utilizes phase cancellation techniques for reducing both the in-band and out-of-band Radar Cross Section (RCS). The structure consists of two substrates with three layers, the top layer consists of 8 antenna elements along with AMCs which are aperiodically oriented for wideband RCS reduction, and the middle layer (in between the two substrates) consists of a corporate feed network for the antenna array, followed by the ground plane in the bottom layer. Few AMC blocks have been used to achieve a wideband RCS reduction in the frequency range of 6 GHz to 16 GHz with more than 85% reduction in both X- and Y-polarizations utilizing a low profile, compact design. Along with the monostatic RCS reduction, a bistatic RCS reduction up to 40° has also been observed in simulations. The proposed structure has been fabricated and measurements of the reflection coefficient, gain, patterns, and monostatic RCS plots have been carried out. Measured results indicate good agreement with the results of the simulations after considering all measurement errors.

INDEX TERMS AMC metasurface, antenna array, multi-layer structure, RCS reduction, stealth technology, wideband.

I. INTRODUCTION

One of the principles of stealth technology is the decrease of the RCS of the target. The RCS is often reduced by applying various coatings or radar-absorbent materials to the fighter aircraft's metallic surface. The opponent radar emits electromagnetic (EM) waves that are directed toward the airborne antennas mounted on aircraft, used for communication purposes with the ground station. These fighter aircraft, unmanned aircraft (drones), and cruise missiles generate the majority of the RCS for stealth operations due to their airborne antennas for signal transmission and reception. So, antenna RCS reduction is very necessary for stealth technology [1].

There have been a few different methods proposed for reducing antenna RCS, such as the shaping of antenna structure, in which the configuration can be reshaped to reflect the EM wave away from the direction in which it was incident [2]. Then, radar-absorbing materials, are also used for antenna RCS reduction [3], [4]. The EM wave can be absorbed by the material, and its energy is converted into heat in this case. Conventional antenna RCS reduction methods, on the other hand, can result in a reduction in antenna radiation performance, such as radiation efficiency, and gain [5]. RCS of low-profile antennas can also be decreased by using frequency selective surfaces (FSS) etc

The associate editor coordinating the review of this manuscript and approving it for publication was Muhammad Usman Afzal.

[6], [7]. The designed FSS sheet operates as a plate in the antenna operating band, ensuring radiation performance, and, outside of the working band, this periodic structure exhibits low scattering and bandpass qualities [8], [9]. The techniques covered in the aforementioned papers are intended to reduce RCS in a limited bandwidth.

For wideband RCS reduction, the chessboard metasurface is created by using two AMC unit cells, incorporated with antennas for RCS reduction [10], while the chessboard configuration discussed in [11] used the unit cell of combined AMC and Perfect Electric Conductor(PEC) (as a checkerboard structure). At the working frequency, the PEC unit cells reflect incident waves with a 180° phase shift, whereas the AMC unit cells provide no phase change to the reflected wave. When these two effects are combined, the bore-sight direction is subjected to destructive interference, and the power is reflected in various directions. But the chessboard configuration has its limitations because of the narrow band. Thus, by substituting another AMC structure for the PEC cell, which operates at a distinct resonance frequency, these narrow band constraints have been eliminated. This substitution creates a destructive interference scenario with a broadband response [12]. To further expand the bandwidth of RCS reduction, three AMC unit cells based on the concept of cascade connection have been proposed. Then, to enable polarization-independent RCS reduction, the metasurface has been designed in a triangular chessboard pattern [13]. To further broaden the bandwidth of RCS reduction, a metasurface design known as a blended checkerboard that combines four AMC unit cells is discussed in [14].

Similarly, electromagnetic band gap (EBG) structures within their band gap must function as AMC unit cells [15]. The polarization conversion metasurface (PCM) used one unit cell cluster and the mirror effect of the same cluster to produce a 180° phase difference. The PCM redirects the back-scattered energy in off-normal directions, thereby reducing the monostatic RCS in near-normal directions [16], [17], [18].

When it comes to military applications, having an antenna with a low RCS is important, but having one with a good gain across a wideband of frequencies is equally necessary. When designing an antenna with a high gain, the aperture size of the antenna must be larger than the size of any individual antenna structure. The RCS of the entire structure will thus automatically rise as a result. Partially reflecting surface (PRS) is a well-known example of a larger aperture size antenna array [19]. A wideband RCS reduction with a higher gain antenna application is given in [20] and [21]. By using a coding metasurface, the RCS has been reduced to a fabry-perot antenna, which has a highly directive beam [22]. However, any form of high-gain antenna application that uses a PRS for enhancing gain requires that the PRS function as a superstate. This results in an increase in the height of the whole structure as well as an increase in the bulkiness of the structure.

In this article, a wideband, 8-element linear patch antenna array has been designed for a narrow-beam directive application with a wideband RCS reduction of more than 85% in X and Y-polarizations. A technique has been used for RCS reduction without extending the antenna structure further for the placement of AMC blocks. This design utilizes two substrates, which results in multi-layer printed circuit boards. The antenna and AMC blocks are placed on the upper substrate, and the feed network is placed on the lower substrate. To make the connection between the top layer antenna and the feed network, eight vias have been constructed.

The main contributions of this work are stated as follows:

- Without increasing the antenna footprint further for the positioning of AMC unit cells, a wideband RCS reduction has been observed for both in-band and out-of-band polarizations. In addition, this structure has a low profile, is simple to implement, and increases radiation efficiency by employing fewer AMC blocks.
- First periodic and subsequently aperiodic orientations have been employed to change and minimize the grating lobes that appear in a certain direction in the case of the periodic structure of the RCS reduction.
- For oblique incident waves (up to 40°), the performance of the antenna remains almost the same, with a substantial RCS reduction in both TE and TM polarizations.

When space is the primary limitation for the placement of a large X-band metasurface antenna that is undetectable by adversary radar on fighter aircraft and missiles, this type of compact antenna will be the best option for application purposes in the advancement of radar stealth technology.

The organization of the paper is as follows: Section II provides details on both AMC structures as well as their magnitude and phase plots. Section III describes the antenna array in detail and the array with AMC metasurface, while Section IV describes the simulated results, followed by Section V, which includes fabrication and measured plots. Finally, in Section VI, concluding remarks have been added.

II. SELECTION OF ARTIFICIAL MAGNETIC CONDUCTORS

10 dB RCS reduction over broadband by using a conventional checkerboard configuration using two AMC unit cells can be determined by equation (1) [23]

$$RCS\ Reduction = 10\log_{10}\left|\frac{A_1 e^{iP_1} + A_2 e^{iP_2}}{2}\right|^2 \quad (1)$$

where, A_1 and A_2 represent the reflection magnitude of the designed AMC unit cells, and reflection phases of AMC unit cells are represented by P_1 and P_2 respectively. The average of the total reflection coefficient is taken into account for the metasurface because both AMC structures occupy exactly half of the whole surface. For 10 dB RCS reduction, the reflection phase difference between two AMC structures is estimated to be $180° \pm 37°$. Destructive interference for RCS

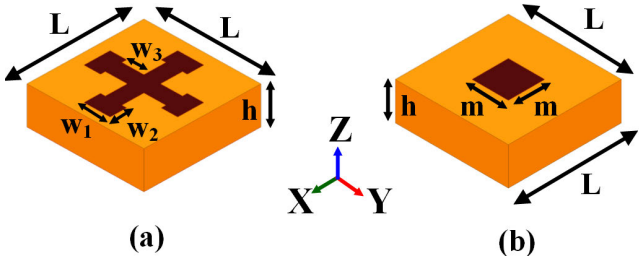

FIGURE 1. Design of AMC unit cells, (a) AMC1, (b) AMC2; where, $L = 9$ mm, $h = 3.5$ mm, $m = 2.1$ mm, $W_1 = 1.73$ mm, $W_2 = 1.1$ mm, $W_3 = 2.37$ mm.

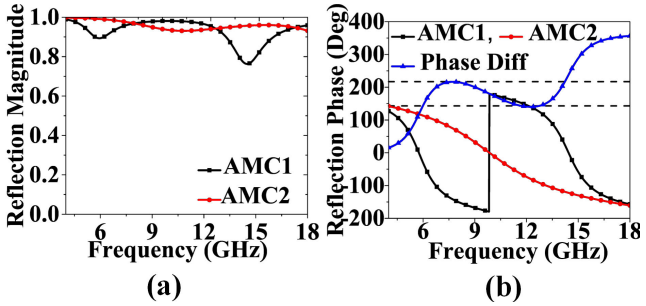

FIGURE 2. (a) Reflection magnitude, (b) phase of the two AMC cells and their phase difference.

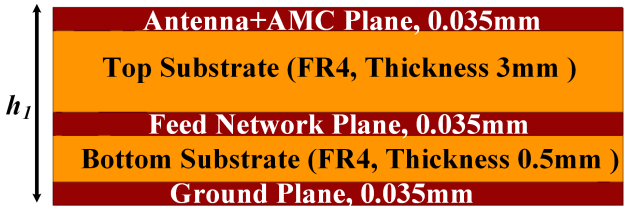

FIGURE 3. Structural orientation details of the antenna array.

reduction is provided by the reflection phase of AMC and PEC unit cells in a checkerboard configuration, although with limited bandwidth. As a result, two AMC unit cells are selected for broadband RCS reduction: one single-band AMC unit cell and one dual-band AMC unit cell, each working at a different resonance frequency. This modification enables compliance with the destructive interference criterion at the resonance frequency of both AMC unit cells.

Therefore, two AMC unit cells have been developed here to create a blended surface with the antenna elements in order to reduce broadband RCS. Two designed AMC unit cells are shown in Fig. 1 along with all of their designed specifications. The idea of the designed AMC unit cells is similar to the AMC structures mentioned in [12] and [24].

For single-band AMC, a simple square patch of FR4 substrate backed by a ground plane is chosen. The reflection magnitude of 0.95 remains constant from 6 GHz to 18 GHz, with a 0° reflection phase at 9.85 GHz. For dual band AMC, a Jerusalem cross with 0° phase reflection at 5.76 GHz and 14.7 GHz and 180° phase reflection at 9.85 GHz has been designed, shown in Fig. 2.

In this case, the reflection magnitude is nearly 0.95 from 6 GHz to 14.7 GHz and 0.98 at 10 GHz, implying total reflection without absorption. The difference between the phases of these two AMC unit cells maintains a wideband from 5.9 GHz to 14.7 GHz for wideband RCS reduction, as shown by the shaded region in Fig. 2.

III. DESIGN OF LINEAR PATCH ANTENNA ARRAY

A. #ANTENNA1

For directive application and to achieve more gain, an 8-element linear microstrip patch antenna array at the X-band has been designed. For antenna elements, FR4 substrate with a loss tangent of 0.02 and permittivity of 4.4 has been chosen for a wideband behavior with a dielectric height (h_a) of 3 mm. The feed network has been designed on the bottom substrate of FR4 having a height of 0.5 mm. The feed network is connected to the patch antennas through copper vias. Usually, a corporate feed involves the connection of a coaxial connector to a vertical transmission line with an impedance of 50 Ω. Subsequently, the network should be further separated into two segments, each consisting of a 100 Ω transmission line. The connection between the 100 Ω line and the next 50 Ω line necessitates the use of a 70 Ω as $\sqrt{(100 \times 50)}$ quarter wave transformer line. In this study, the authors have selected a substrate with a thickness of 0.5 mm made of FR4 material, which possesses a loss tangent of 0.02 and a permittivity value of 4.4. Based on the given substrate, the width of the 100 Ω line is determined to be 0.19 mm, which is very thin to fabricate. Instead of utilizing that microstrip line, the authors have opted for a direct connection between a 70 Ω line and 50 Ω lines as discussed in [25]. This feed network with eight patch elements is named #Antenna1. The structural orientation is shown in Fig. 3.

The antenna array provides 11.5 dB of realized gain and the bandwidth is from 7.8 GHz to 12.1 GHz, except 11.14 to 11.4 GHz in which return loss is below 9.5 dB with more than 36% bandwidth. Antenna design results in greater additional dielectric losses since a thicker substrate is chosen. As a result, the quality factor is lower, and since bandwidth and Q-factor are inversely related, bandwidth is wider. The length, L_1 is 112 mm, the width, L_2 is 58 mm and the total height of the full structure is h_1 3.5 mm, shown in Fig. 4(a).

From the standpoint of scattering, it is important to note that, as with a single antenna, the RCS of an antenna can be composed of an antenna component and a structural term shown in the below equation (2) [26], [27].

$$\sigma = \left|\sqrt{\sigma_{Structural}} - (1 - \Gamma_a)\sqrt{\sigma_{Antenna}}\, exp^{\varphi_{rel}}\right|^2 \quad (2)$$

Here, σ designates the total RCS of the structure, where $\sigma_{Structural}$ denotes the scattered field by the short-circuited antenna, $\sigma_{Antenna}$ denotes the scattered field by the antenna which has some port impedance values, φ_{rel} represents the relative phase between $\sigma_{Structural}$ and $\sigma_{Antenna}$, and Γ_a represents the reflection coefficient due to mismatch of the antenna. A short circuit condition is defined as $\Gamma_a = 1$, which

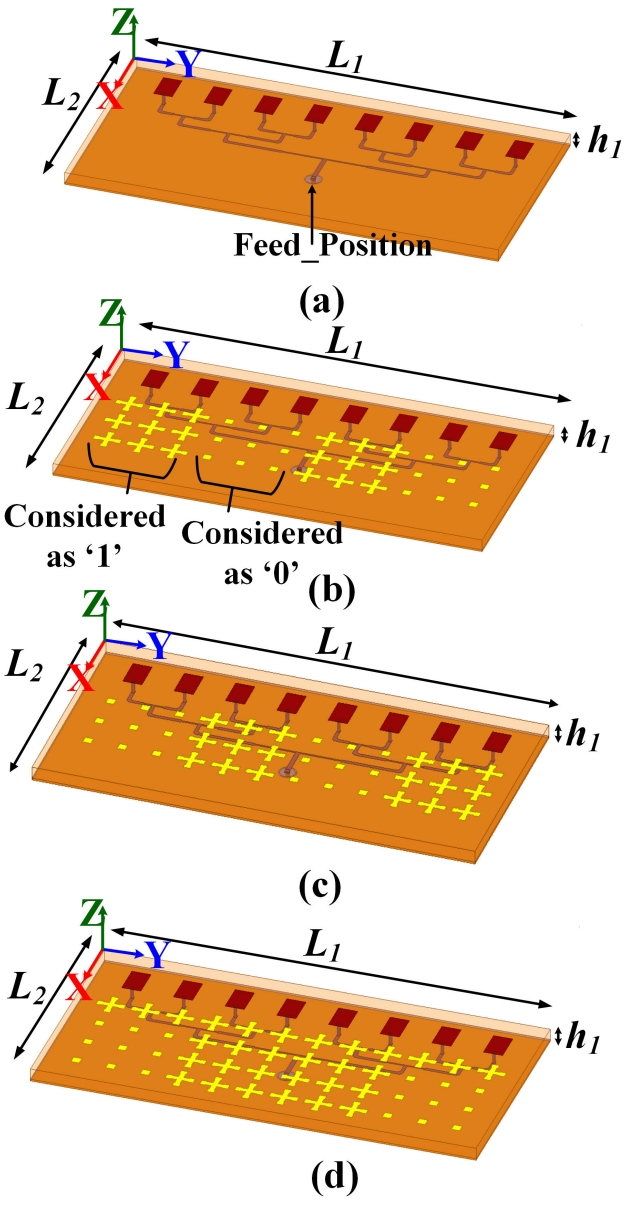

FIGURE 4. 8-elements patch array (a) #Antenna1, (b) #Antenna2, (c) #Antenna3, (d) #Antenna4.

makes equation (2) as,

$$\sigma_{short} = \sigma_{structure} \tag{3}$$

Similarly, an open-circuited condition is defined as $\Gamma_a = -1$, which makes equation (2) as,

$$\sigma_{open} = \left|\sqrt{\sigma_{Structural}} - 2\sqrt{\sigma_{Antenna}}\, exp^{\varphi_{rel}}\right|^2 \tag{4}$$

and at last matched is defined as $\Gamma_a = 0$ gives

$$\sigma_{match} = \left|\sqrt{\sigma_{Structural}} - \sqrt{\sigma_{Antenna}}\, exp^{\varphi_{rel}}\right|^2 \tag{5}$$

As the worst-case scenario suggests, the primary objective of this paper is to decrease RCS under short-circuit conditions. Even though it would be obvious that the RCS has decreased in comparison to both the matched condition and the metal plate.

For the reduction of RCS, three types of metasurface antenna array have been designed, named #Antenna2, #Antenna3, and #Antenna4 by using the previously discussed two AMC structures. The blocks of AMC1 using 3×3 unit cells are named '1' and the blocks of AMC2 using 3×3 unit cells are named '0'.

B. #ANTENNA2

Only four blocks of AMC structures oriented as '1', and '0' periodicity have been used with #Antenna1 for RCS reduction. The AMC blocks are placed at the top layer of the top substrate along with antenna elements, shown in Fig. 4(b). The reflection coefficient of this structure provides a wideband response from 7.4 GHz to 11.45 GHz with a realized gain of 10.95 dB. The total length L_1, width L_2 and height h_1 is same as that of #Antenna1. The AMC blocks adjacent to antenna elements are not identical due to the periodicity of the metasurface, which results in an asymmetric side lobe level radiation pattern.

C. #ANTENNA3

Like #Antenna2, #Antenna3 has also been designed by using the same four blocks of AMC structures but with different periodicity, maintaining '0', '1' orientation with #Antenna1 for RCS reduction, shown in Fig. 4(c). The reflection coefficient of this structure also provides a wideband of 7.47 GHz to 11.53 GHz with a realized gain of 10.99 dB. Due to the orientation of two different types of AMC blocks next to the antenna components, there is pattern asymmetry at the first side lobe level in this instance as well.

D. #ANTENNA4

Aperiodicity is used in the case of #Antenna4 to change the pre-determined direction of grating lobes that results from the periodic structure in order to increase the scattering performance of the metasurface antenna. This is done because the grating lobe theory mentioned in [12] determines the scattering direction of periodic structures.

By using 3×3 AMC blocks, only two aperiodic structures can be created, either maintaining '0', '1', '1', '0' orientation or '1', '0', '0', and '1' orientation. So, by using four blocks of AMC structures, maintaining aperiodicity as '0', '1', '1', and '0' orientation followed by one single layer of AMC1 at the top of 4 AMC blocks with #Antenna1, #Antenna4 has been designed, shown in Fig. 4(d). One single layer of AMC1 has been added to maintain the symmetry of side lobe levels. This leads to a gain enhancement of 1.2 dB with an equal side lobe that is similar to the original radiation pattern. The reflection coefficient of this structure also provides a wideband of 7.7 GHz to 11.6 GHz with a realized gain of 12.25 dB.

IV. ANTENNA RADIATION AND SCATTERING PERFORMANCE WITH SIMULATED RESULTS

The task of reducing the RCS of an array antenna presents a trade-off between increasing system complexity and dete-

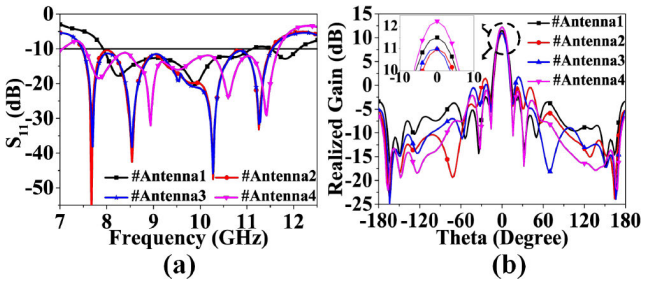

FIGURE 5. (a) Simulated reflection coefficient plots of all antennas (b) 2D radiation pattern at $\phi = 90°$ of all configurations of antennas with realized gain.

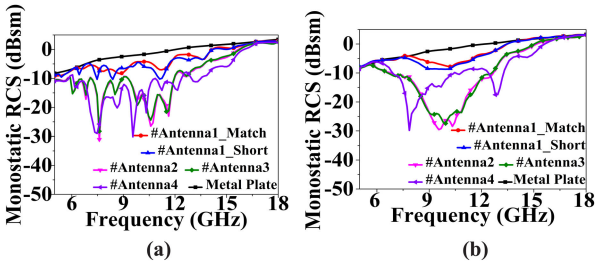

FIGURE 6. Monostatic RCS plot in (a) Y-polarization and (b) X-polarization.

riorating the array's radiation performance. Remembering both aspects, the antenna arrays have been proposed with a minimum number of AMC blocks to reduce system complexity, and as this is a wideband antenna array, the antenna will receive incident power throughout its band.

A. RADIATION PERFORMANCE

The proposed four types of antennas have been simulated in Ansys HFSS software and the simulated results of all antennas have been shown and discussed in this section. As stated about the wideband nature of four antennas in the last section, the S_{11} plot of 4 configurations of antennas has been shown in Fig. 5(a), and the 2D radiation pattern with the realized gain plot of four configurations of antennas have been shown in Fig. 5(b) which shows a proper gain enhancement of #Antenna4 with respect to #Antenna1.

B. SCATTERING PERFORMANCE

For RCS reduction, normal incident wave and oblique incident wave on the antenna arrays have been observed and shown here.

1) NORMAL INCIDENT WAVE

The monostatic RCS plot of X-polarization and Y-polarization under the normal incident wave of a same-sized metal plate, antenna array named as #Antenna1 with the shorted condition, #Antenna1 with the matched condition, #Antenna2, #Antenna3, #Antenna4 have been shown in Fig. 6. As the antenna array is a wideband antenna, so it accepts or receives more power throughout the band either in shorted or matched conditions.

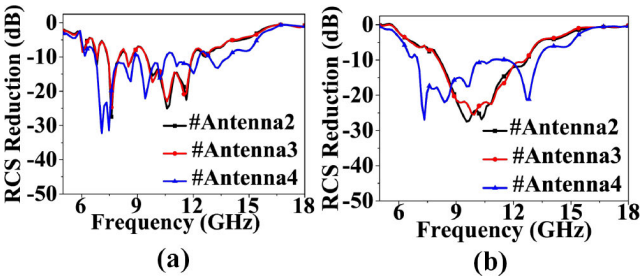

FIGURE 7. Monostatic RCS reduction in (a) Y-polarization (b) X-polarization w.r.t. metal plate.

A significant amount of RCS reduction for both polarizations has been obtained from 6 GHz to 15 GHz in all cases.

By applying a matched load of 50 Ω impedance to the feed port, the monostatic RCS has been obtained to determine the antenna component effect. It may be assumed that the antenna component has little influence on RCS modifications outside of the working bandwidth and is functioning almost like a PEC because the only significant RCS fluctuation is observed around the antenna's resonant frequency or across the antenna's working bandwidth.

Because of this, the RCS reduction from a metal plate of the same size has been properly demonstrated, providing very significant RCS reduction in all antenna configurations and a very wideband for #Antenna4 with over 10 dB RCS reduction across the band of 6 GHz to 15 GHz. Fig. 7(a) and (b) display monostatic RCS reduction plots for both polarizations relative to a metal plate.

By comparing the monostatic RCS reduction for both the polarizations depicted in the figures, it is obvious that all the proposed configurations have a lower radar cross-section than the original microstrip antenna array, with up to a maximum 30 dB of reduction for #Antenna2, #Antenna3, and #Antenna4 by using fewer numbers of AMC blocks. While #Antenna2 and #Antenna3 provide more RCS reduction throughout the X-band, the #Antenna4 provides RCS reduction in some portions of the C-and Ku-bands and covers a full band of X-band. Table. 1 show the average RCS reduction of all the configurations of the antennas with respect to shorted #Antenna1.

2) OBLIQUE INCIDENT WAVE

Up to an incident angle of 40°, the RCS of the proposed antenna configurations is also studied and presented here. The surface impedance of the AMC metasurface depends on the angle of incidence. As a result, the impedance of the incoming wave varies with respect to the angle at which it is arriving. As a result, the phase of reflection for both polarizations changes [28]. Because of this, a frequency shift happens within the same band as the normal incident wave.

Considering the worst case for RCS reduction, it has been observed that a significant amount of RCS has been reduced even in the case of specular direction for the proposed antenna. Fig. 8(a) and (b) show the bistatic RCS

TABLE 1. Average RCS reduction of All antenna configurations.

RCS Reduction w.r.t. Shorted Antenna Array			
Antenna Configuration	Frequency Range (GHz)	Average Monostatic RCS Reduction (dB)	
		x-Pol	y-Pol
#Antenna2	6-15	7.06	8.37
#Antenna3	6-15	6.84	8.78
#Antenna4	6-15	7.61	8.08
RCS Reduction w.r.t. Metal Plate (same size of antenna)			
Antenna Configuration	Frequency Range (GHz)	Average Monostatic RCS Reduction (dB)	
		x-Pol	y-Pol
#Antenna2	6-15	9.76	10.85
#Antenna3	6-15	9.58	10.52
#Antenna4	6-15	11.34	11.38

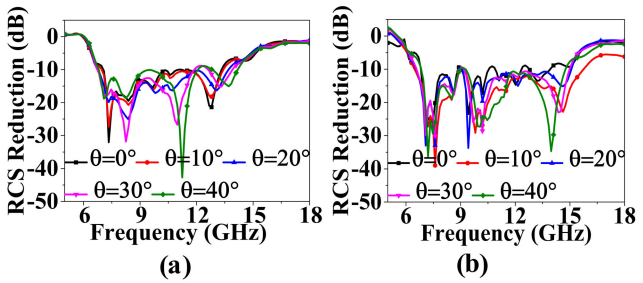

FIGURE 8. Specular RCS reduction in (a) TM and (b) TE polarization up to 40° of #Antenna4 w.r.t. metal.

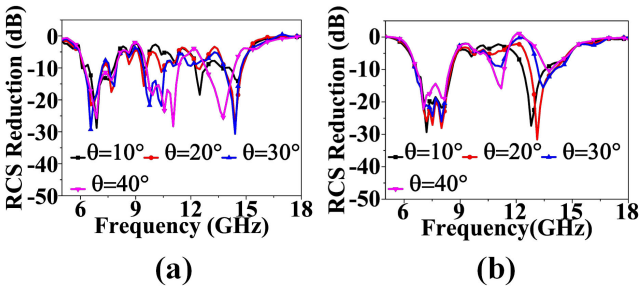

FIGURE 9. Specular RCS reduction in (a) TM and (b) TE polarization up to 40° of #Antenna4 w.r.t. shorted #Antenna1.

plot #Antenna4 in TM polarization and TE polarization with respect to the metal plate of similar size.

Fig. 9(a) and (b) show the bistatic RCS plot of #Antenna4 in TM and TE polarization compared to #Antenna1 in shorted condition.

It is not surprising that as the reflection phase varies as a function of the incident angle, the average RCS reduction bandwidth narrows. But in the situation of aperiodic structure, which causes an aperiodic reduction in RCS, as shown in Table 2, the same effect does not apply. This is because the same phenomenon does not occur at regular intervals.

C. 3D RCS PLOTS

The phase behavior of the AMC structure depends on the incidence angle of the plane wave, which constrains the scattering behavior of the checkerboard patterns and results in the production of grating lobes. For three configurations

TABLE 2. Average specular RCS reduction of all antenna configurations.

Antenna	Average Specular RCS Reduction (dB)			
	TM Polarization			
	$\theta = 10°$	$\theta = 20°$	$\theta = 30°$	$\theta = 40°$
#Antenna2	7.8	7.4	6.21	5.94
#Antenna3	7.96	7.24	6.08	5.99
#Antenna4	8.1	8.76	10.1	10.96
	TE Polarization			
	$\theta = 10°$	$\theta = 20°$	$\theta = 30°$	$\theta = 40°$
#Antenna2	8.73	8.31	7.43	6.37
#Antenna3	8.93	8.84	7.45	5.97
#Antenna4	8.77	9.04	7.96	6.92

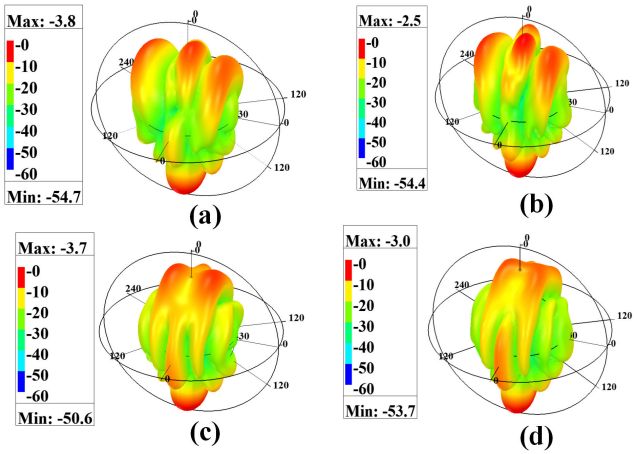

FIGURE 10. 3D RCS plot of #Antenna2 and #Antenna4 at X-polarization, (a) #Antenna2 at 8 GHz, (b) #Antenna2 at 9 GHz, (c) #Antenna4 at 8 GHz, (d) #Antenna4 at 9 GHz.

at various frequencies, 3D RCS plots are provided below to illustrate the scattering direction of metasurface antennas.

Fig. 10(a), (b), and 11(a), (b) show the 3D RCS plot of #Antenna2 under normal incident wave for X-and Y-polarization respectively for the frequency of 8 GHz and 9 GHz, and Fig. 10(c), (d), and 11(c), (d) show the 3D RCS plot of #Antenna4 under normal incident wave for X- and Y-polarization, respectively, for the frequencies of 8 GHz and 9 GHz.

According to the array theory, the grating lobes that are generated by the periodic metasurface, i.e., #Antenna2 and #Antenna3 which use periodic AMC blocks, are fixed. However, any prominent grating lobe does not occur in the case of #Antenna4. This can be seen quite clearly from the 3D RCS plots that have been shown above. Even though only two frequency plots are displayed here, this logic holds for the entire frequency range that is described.

V. FABRICATION AND MEASUREMENTS

After the structures have been simulated, #Antenna4 has been fabricated and measured, as shown in Fig. 12, as the #Antenna4 provides wide RCS reduction bandwidth and improves the radiation and scattering properties of the antenna w.r.t. #Antenna1. The antenna has been fabricated using two substrates. The upper substrate contains an AMC metasurface and antenna elements, which are connected

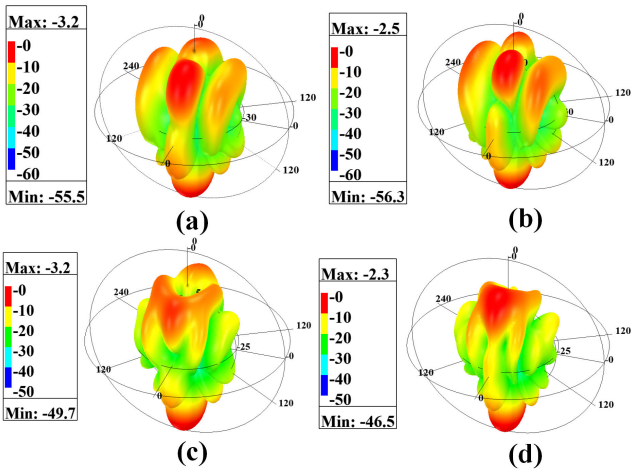

FIGURE 11. 3D RCS plot of #Antenna2 and #Antenna4 at Y-polarization, (a) #Antenna2 at 8 GHz, (b) #Antenna2 at 9 GHz, (c) #Antenna4 at 8 GHz, (d) #Antenna4 at 9 GHz.

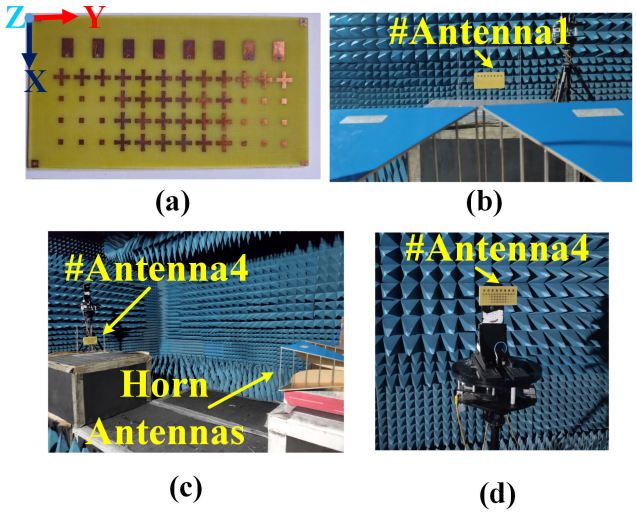

FIGURE 12. (a) fabricated structure, #Antenna4 and (b) RCS measurement setup of #Antenna1, (c) RCS measurement setup of #Antenna4, and (d) pattern measurements setup of the #Antenna4.

with the feed network in the lower substrate through PTH vias. Then a coaxial SMA connector has been used from the backside to feed the antenna. The two substrates of FR4 have been pasted using epoxy resin and a hard press technique to minimize the air gap between the two substrate layers.

Fig. 13(a) shows good agreement between the S_{11} simulated and measured results across the entire X-band. The measured S_{11} provides a wideband of 44% bandwidth covering from 7.43 GHz to 11.7 GHz. The S_{11} has been measured using Agilent PNA N5222A.

After the S_{11}, the radiation pattern and scattering permanence of #Antenna4 have been measured in an anechoic chamber. A plot of the realized gain versus frequency is shown in Fig. 13(b). While the simulated realized gain was 12.25 dB, the highest measured gain is 11.95 dB. The radiation pattern in the YZ plane and XZ plane has

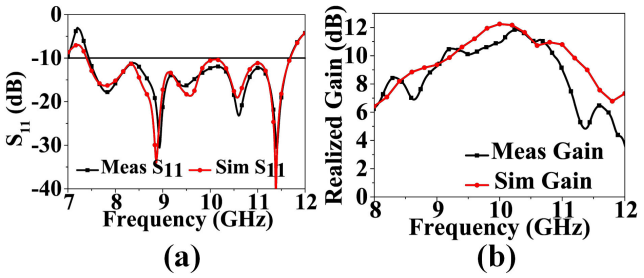

FIGURE 13. (a) Simulated and measured S_{11} of #Antenna4 and (b) simulated and measured realized gain of #Antenna4.

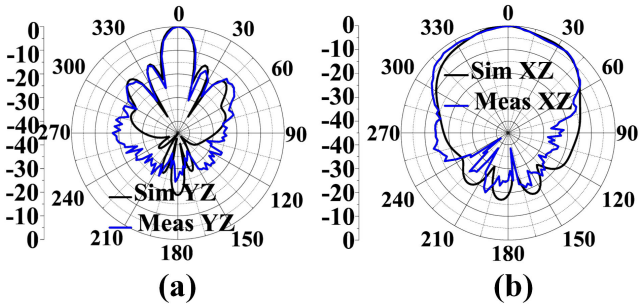

FIGURE 14. 2D Radiation pattern (simulated and measured) of #Antenna4 (a) YZ plane and (b) XZ plane.

TABLE 3. Measured average RCS reduction (From 6 GHz to 16 GHz).

Avg. RCS reduction (Measured)	X-pol	Y-pol
w.r.t. #Antenna1	-5.49 dB	-5.83 dB
w.r.t. Metal	-9.29 dB	-11.63 dB

been measured and plotted with the simulated radiation pattern, which shows good agreement with each other as shown in Fig. 14. The differences between measured and simulated results are acceptable when fabrication tolerances and measurement deviations, such as antenna misalignment, and the use of epoxy resin for hard pressing of the structure, are taken into account.

For scattering performance, the two-horn antenna method has been used for monostatic RCS reduction measurements. To emphasize the low-RCS feature of the proposed array, the RCS of a reference array with identical 8 patch antennas and an identical-sized metal board is also measured.

Fig. 15 shows a proper RCS reduction between the band of 6 GHz to 16 GHz w.r.t. a metal plate and from 7 GHz to 18 GHz w.r.t. a matched reference antenna array. The measured average RCS reduction of both cases has been shown in Table 3. There are differences between the simulated and measured findings in the RCS reduction plot. The incident wave impinging on the surface in simulations is considered a perfect plane wave, but the horn aperture's far-field radiation is hardly consistent with a typical plane wave, which results in the differences.

Despite choosing a lossy, low-cost substrate, the proposed work offers a wide RCS reduction bandwidth, higher gain, smaller size, and higher impedance bandwidth when com-

TABLE 4. Comparison table.

Reference	Antenna Frequency Range (GHz) Bandwidth (%)	In band RCS reduction	RCS Reduction Range (GHz), %	Gain (dBi)	Antenna Elements	Size (mm^2) (w.r.t. centre freq of antenna)
[10]	9.6-11.4	Yes	8.8-17.3, 65%	8.1	1	81×81
	17%					$2.83\lambda \times 2.83\lambda$
[29]	5.48-5.84	Yes	4.95-7.18, 36%	9.5 (From Fig.)	1	120×120
	6%					$2.24\lambda \times 2.24\lambda$
[30]	5.42-5.84	Yes	4.35-7.8, 56%	9.5(From Fig.)	1	120×120
	7%					$2.25\lambda \times 2.25\lambda$
[31]	3.16-3.36	Yes	2.85-3.95, 32%	11 (From Fig)	1	313×313
	6%					$3.39\lambda \times 3.39\lambda$
[32]	4.3-5.1	Yes	4.53-6.7, 42%	15.6	4×4	160×160
	17%					$2.67\lambda \times 2.67\lambda$
[33]	2.99-3.16	No	6-13.4, 72%	14.13	2×2	180×180
	5%					$1.8\lambda \times 1.8\lambda$
[34]	10.4-11.2	Yes	9.5-26, 92%	9.1	5	78×104
	9%					$3.74\lambda \times 2.81\lambda$
[35]	4.7-6.95	Yes	4.7-5.8, 20%	12.7 (Max)	2×2	92×92
	38%					$1.81\lambda \times 1.81\lambda$
[36]	9.66-11.38	Yes	9.2-18.9, 69%	8 (Max)	1	81×81
	16%					$2.83\lambda \times 2.83\lambda$
[37]	9.2-12	Yes	7.4-11.9, 46%	7.8	1	63×63
	26%					$2.1\lambda \times 2.1\lambda$
[38]	14.2-15.5	Yes	9.3-28.2 (Sim), 100% 9.2-18 (Meas), 64%	7.3	1	80×80
	8.75%					$2.48\lambda \times 2.48\lambda$
[39]	32-33	Yes	29.5-50, 51.5%	7	1	25×25
	3%					$2.75\lambda \times 2.75\lambda$
This Work	**7.43-11.7**	**Yes**	**6-16, 90%**	**11.95**	**8**	$\mathbf{58 \times 112}$
	44%					$\mathbf{1.84\lambda \times 3.55\lambda}$

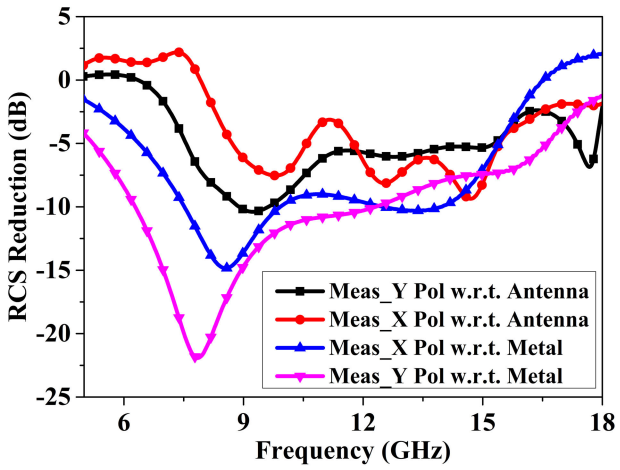

FIGURE 15. Measured monostatic RCS reduction plot of #Antenna4 w.r.t.#Antenna1 and metal plate.

pared to low-scattering metasurface-based antennas found in the literature, as shown in Table 4.

VI. CONCLUSION

A linear microstrip patch antenna array with a wide band and more directive gain has been designed with fewer numbers of AMC blocks for RCS reduction over a wideband without extending the size of the array further. At first, a periodic and then an aperiodic metasurface has been designed to change the direction of the grating lobes generated by the periodic metasurface. While the bottom layer consists of a feed network, the top layer contains the patch elements and AMC blocks which make this structure very compact and smaller in size. Based upon the simulation results the antenna array with aperiodic metasurface, named #Antenna4, has been fabricated and measured. Reflection coefficient, radiation patterns, gain, and monostatic RCS patterns have been measured and tabulated, which show a very good agreement with simulation results. So, the proposed low RCS antenna array can be easily used for stealth technology and radar applications.

REFERENCES

[1] D. M. Pozar, "RCS reduction for a microstrip antenna using a normally biased ferrite substrate," *IEEE Microw. Guided Wave Lett.*, vol. 2, no. 5, pp. 196–198, May 1992.
[2] Y. B. Thakare, "Design of fractal patch antenna for size and radar cross-section reduction," *IET Microw., Antennas Propag.*, vol. 4, no. 2, pp. 175–181, Feb. 2010.
[3] N. Engheta, "Thin absorbing screens using metamaterial surfaces," in *Proc. IEEE Antennas Propag. Soc. Int. Symp.*, Mar. 2002, pp. 392–395.
[4] Q. Gao, Y. Yin, D.-B. Yan, and N. C. Yuan, "Application of metamaterials to ultra-thin radar-absorbing material design," *Electron. Lett.*, vol. 41, no. 17, pp. 936–937, Aug. 2005.
[5] Y. Jia, Y. Liu, H. Wang, K. Li, and S. Gong, "Low-RCS, high-gain, and wideband mushroom antenna," *IEEE Antennas Wireless Propag. Lett.*, vol. 14, pp. 277–280, 2015.
[6] S. Genovesi, F. Costa, and A. Monorchio, "Low-profile array with reduced radar cross section by using hybrid frequency selective surfaces," *IEEE Trans. Antennas Propag.*, vol. 60, no. 5, pp. 2327–2335, May 2012.
[7] J. P. Turpin, P. E. Sieber, and D. H. Werner, "Absorbing ground planes for reducing planar antenna radar cross-section based on frequency selective surfaces," *IEEE Antennas Wireless Propag. Lett.*, vol. 12, pp. 1456–1459, 2013.
[8] N. Misran, R. Cahill, and V. Fusco, "RCS reduction technique for reflectarray antennas," *Electron. Lett.*, vol. 39, pp. 1630–1632, Dec. 2003.

[9] W.-T. Wang, S.-X. Gong, X. Wang, H.-W. Yuan, J. Ling, and T.-T. Wan, "RCS reduction of array antenna by using bandstop FSS reflector," *J. Electromagn. Waves Appl.*, vol. 23, nos. 11–12, pp. 1505–1514, Jan. 2009.

[10] Y. Zheng, J. Gao, X. Cao, Z. Yuan, and H. Yang, "Wideband RCS reduction of a microstrip antenna using artificial magnetic conductor structures," *IEEE Antennas Wireless Propag. Lett.*, vol. 14, pp. 1582–1585, 2015.

[11] M. Paquay, J.-C. Iriarte, I. Ederra, R. Gonzalo, and P. de Maagt, "Thin AMC structure for radar cross-section reduction," *IEEE Trans. Antennas Propag.*, vol. 55, no. 12, pp. 3630–3638, Dec. 2007.

[12] J. C. I. Galarregui, A. T. Pereda, J. L. M. de Falcón, I. Ederra, R. Gonzalo, and P. de Maagt, "Broadband radar cross-section reduction using AMC technology," *IEEE Trans. Antennas Propag.*, vol. 61, no. 12, pp. 6136–6143, Dec. 2013.

[13] Y. Zheng, J. Gao, L. Xu, X. Cao, and T. Liu, "Ultrawideband and polarization-independent radar-cross-sectional reduction with composite artificial magnetic conductor surface," *IEEE Antennas Wireless Propag. Lett.*, vol. 16, pp. 1651–1654, 2017.

[14] A. Y. Modi, C. A. Balanis, C. R. Birtcher, and H. N. Shaman, "Novel design of ultrabroadband radar cross section reduction surfaces using artificial magnetic conductors," *IEEE Trans. Antennas Propag.*, vol. 65, no. 10, pp. 5406–5417, Oct. 2017.

[15] J. Zhang, J. Wang, M. Chen, and Z. Zhang, "RCS reduction of patch array antenna by electromagnetic band-gap structure," *IEEE Antennas Wireless Propag. Lett.*, vol. 11, pp. 1048–1051, 2012.

[16] Y. Liu, K. Li, Y. Jia, Y. Hao, S. Gong, and Y. J. Guo, "Wideband RCS reduction of a slot array antenna using polarization conversion metasurfaces," *IEEE Trans. Antennas Propag.*, vol. 64, no. 1, pp. 326–331, Jan. 2016.

[17] Y. Liu, Y. Hao, K. Li, and S. Gong, "Radar cross section reduction of a microstrip antenna based on polarization conversion metamaterial," *IEEE Antennas Wireless Propag. Lett.*, vol. 15, pp. 80–83, 2016.

[18] K. Li, Y. Liu, Y. Jia, and Y. J. Guo, "A circularly polarized high-gain antenna with low RCS over a wideband using chessboard polarization conversion metasurfaces," *IEEE Trans. Antennas Propag.*, vol. 65, no. 8, pp. 4288–4292, Aug. 2017.

[19] A. P. Feresidis, G. Goussetis, S. Wang, and J. C. Vardaxoglou, "Artificial magnetic conductor surfaces and their application to low-profile high-gain planar antennas," *IEEE Trans. Antennas Propag.*, vol. 53, no. 1, pp. 209–215, Jan. 2005.

[20] W. Pan, C. Huang, P. Chen, X. Ma, C. Hu, and X. Luo, "A low-RCS and high-gain partially reflecting surface antenna," *IEEE Trans. Antennas Propag.*, vol. 62, no. 2, pp. 945–949, Feb. 2014.

[21] H. Jiang, Z. Xue, W. Li, W. Ren, and M. Cao, "Low-RCS high-gain partially reflecting surface antenna with metamaterial ground plane," *IEEE Trans. Antennas Propag.*, vol. 64, no. 9, pp. 4127–4132, Sep. 2016.

[22] L. Zhang, X. Wan, S. Liu, J. Y. Yin, Q. Zhang, H. T. Wu, and T. J. Cui, "Realization of low scattering for a high-gain Fabry–Pérot antenna using coding metasurface," *IEEE Trans. Antennas Propag.*, vol. 65, no. 7, pp. 3374–3383, Jul. 2017.

[23] W. Chen, C. A. Balanis, and C. R. Birtcher, "Checkerboard EBG surfaces for wideband radar cross section reduction," *IEEE Trans. Antennas Propag.*, vol. 63, no. 6, pp. 2636–2645, Jun. 2015.

[24] P. Yao, B. Zhang, and J. Duan, "A broadband artificial magnetic conductor reflecting screen and application in microstrip antenna for radar cross-section reduction," *IEEE Antennas Wireless Propag. Lett.*, vol. 17, no. 3, pp. 405–409, Mar. 2018.

[25] H. Visser, *Array and Phased Array Antenna Basics*. Hoboken, NJ, USA: Wiley, Feb. 2006.

[26] S. Genovesi, F. Costa, and A. Monorchio, "Wideband radar cross section reduction of slot antennas arrays," *IEEE Trans. Antennas Propag.*, vol. 62, no. 1, pp. 163–173, Jan. 2014.

[27] R. C. Hansen, "Relationships between antennas as scatterers and as radiators," *Proc. IEEE*, vol. 77, no. 5, pp. 659–662, May 1989.

[28] O. Luukkonen, C. Simovski, G. Granet, G. Goussetis, D. Lioubtchenko, A. V. Raisanen, and S. A. Tretyakov, "Simple and accurate analytical model of planar grids and high-impedance surfaces comprising metal strips or patches," *IEEE Trans. Antennas Propag.*, vol. 56, no. 6, pp. 1624–1632, Jun. 2008.

[29] Y. Zhao, X. Cao, J. Gao, X. Yao, and X. Liu, "A low-RCS and high-gain slot antenna using broadband metasurface," *IEEE Antennas Wireless Propag. Lett.*, vol. 15, pp. 290–293, 2016.

[30] Y. Zhao, X. Cao, J. Gao, X. Yao, T. Liu, W. Li, and S. Li, "Broadband low-RCS metasurface and its application on antenna," *IEEE Trans. Antennas Propag.*, vol. 64, no. 7, pp. 2954–2962, Jul. 2016.

[31] Z.-J. Han, W. Song, and X.-Q. Sheng, "Gain enhancement and RCS reduction for patch antenna by using polarization-dependent EBG surface," *IEEE Antennas Wireless Propag. Lett.*, vol. 16, pp. 1631–1634, 2017.

[32] Y. Zhao, X. Cao, J. Gao, L. Xu, X. Liu, and L. Cong, "Broadband low-RCS circularly polarized array using metasurface-based element," *IEEE Antennas Wireless Propag. Lett.*, vol. 16, pp. 1836–1839, 2017.

[33] C. Zhang, J. Gao, X. Cao, L. Xu, and J. Han, "Low scattering microstrip antenna array using coding artificial magnetic conductor ground," *IEEE Antennas Wireless Propag. Lett.*, vol. 17, no. 5, pp. 869–872, May 2018.

[34] X. Ding, Y.-F. Cheng, W. Shao, and B.-Z. Wang, "A planar wide-angle scanning phased array with *X*-, *Ku*-, and *K*-band RCS reduction," *IEEE Trans. Antennas Propag.*, vol. 68, no. 5, pp. 4103–4108, May 2020.

[35] Q. Zheng, C. Guo, G. A. E. Vandenbosch, and J. Ding, "Low-profile circularly polarized array with gain enhancement and RCS reduction using polarization conversion EBG structures," *IEEE Trans. Antennas Propag.*, vol. 68, no. 3, pp. 2440–2445, Mar. 2020.

[36] Y. Zheng, J. Gao, Y. Zhou, X. Cao, L. Xu, S. Li, and H. Yang, "Metamaterial-based patch antenna with wideband RCS reduction and gain enhancement using improved loading method," *IET Microw., Antennas Propag.*, vol. 11, no. 9, pp. 1183–1189, Jul. 2017.

[37] B. Bandyopadhyay, R. K. Jaiswal, and K. V. Srivastava, "In-band RCS reduction of microstrip patch antenna using artificial magnetic conductors at X-band for stealth technology," in *Proc. IEEE Microw., Antennas, Propag. Conf. (MAPCON)*, Dec. 2022, pp. 180–185.

[38] T. Zhang, X. Pang, H. Zhang, and Q. Zheng, "Ultrabroadband RCS reduction and gain enhancement of patch antennas by phase gradient metasurfaces," *IEEE Antennas Wireless Propag. Lett.*, vol. 22, no. 3, pp. 665–669, Mar. 2023.

[39] S. A. M. Soliman, E. M. El-Desouki, S. M. El-Nady, and A. S. A. El-Hameed, "Broadband low RCS based on polarization-dependent artificial magnetic conductor metasurface," *IEEE Access*, vol. 11, pp. 53176–53184, 2023.

BAISAKHI BANDYOPADHYAY (Graduate Student Member, IEEE) received the B.Tech. degree in electronics and communication engineering from the West Bengal University of Technology, India, in 2014, and the Master of Engineering degree from the Birla Institute of Technology Mesra, India, in 2017. She is currently pursuing the Ph.D. degree in RF and microwave with the Indian Institute of Technology Kanpur, India, under the Prime Minister Research Fellowship (PMRF) Program. She did her master's project with the Society for Applied Microwave Electronics Engineering and Research (SAMEER), Kolkata, from 2016 to 2017. Thereafter, she joined Jadavpur University as a Junior Research Fellow in ISRO respond project on waveguide slotted array antenna. Later, she joined as a Project Assistant in Rashtriya Uchchatar Shiksha Abhiyan (RUSA) Project under the Government of India with Jadavpur University. Her work was on channel characterization for 5G systems. She was awarded CSIR-SRF by the Government of India. Her research interests include antenna arrays, metamaterials, metasurface, FSS absorbers, time-modulated metasurface, and RCS reduction techniques. She has worked in various capacities serving as a Webmaster, a Treasurer, and the Vice-Chair of IEEE AP-S and MTT-S SBCs. She is also serving as a Subcommittee Member of the IEEE MTT-S EIC Group.

SUDEB BHATTACHARYA (Graduate Student Member, IEEE) was born in Kolkata, India, in 1996. He received the B.Tech. degree in electronics and communication engineering from the GB Pant Government Engineering College, New Delhi, India, in 2018, and the master's degree from the Microwave Metamaterial Laboratory, Department of Electrical Engineering, Indian Institute of Technology Kanpur, where he is currently pursuing the Ph.D. degree. His research interests include RCS reduction, active metasurfaces, reflective intelligent surfaces, finite difference techniques, and transparent metasurface manufacturing technologies. He served as the Webmaster of IEEE MTTS SBC IIT Kanpur, in 2022. He is also serving as a Treasurer, in 2023.

RAHUL KUMAR JAISWAL (Graduate Student Member, IEEE) is currently pursuing the Doctor of Philosophy (Ph.D.) degree in RF and microwaves discipline with the Electrical Engineering Department, Indian Institute of Technology (IIT) Kanpur, India, under the supervision of Prof. Kumar Vaibhav Srivastava. He was also a Scientist with the Institute for Plasma Research (IPR), Gandhinagar, India. He is an active member of the IEEE Antennas and Propagation Society (AP-S). He has served as the Chair for the IEEE AP-S Student Branch Chapters at IIT Kanpur and he has been awarded the IEEE AP-S Doctoral Research Grant 2021. He is also a recipient of the IEEE UP Section Outstanding Section Student Volunteer Award 2022. His research interests include base station antennas, multi-input multi-output (MIMO) antennas, end-fire circularly polarized antennas, polarization reconfigurable CP antennas, full duplex antennas, and beamforming antennas. He has authored or coauthored over 20 journals and conference papers in these areas.

MONDEEP SAIKIA (Member, IEEE) received the B.Tech. degree in electronics and communication engineering from the National Institute of Technology Silchar, India, in 2013, the M.Tech. degree in electrical engineering from the Indian Institute of Technology (IIT) Kanpur, India, in 2016, and the Ph.D. degree in electrical engineering from IIT Kanpur, in 2023, under the guidance of Prof. Kumar Vaibhav Srivastava. He has accepted a research fellow position with the Center for Wireless Innovation, Queen's University Belfast. He has authored or coauthored 15 peer-reviewed articles in international journals and 17 conference papers. His current research interests include microwave absorbers, frequency-selective surfaces, space–time-modulated metasurfaces, microwave imaging, and polarization rotators. He is also an active member of the IEEE AP Society and IEEE MTT Society.

KUMAR VAIBHAV SRIVASTAVA (Senior Member, IEEE) was born in Allahabad, India, in May 1982. He received the B.Tech. degree in electronics engineering from the Kamla Nehru Institute of Technology, Sultanpur, India, in 2002, and the M.Tech. and Ph.D. degrees in electrical engineering from the Indian Institute of Technology (IIT) Kanpur, Kanpur, India, in 2004 and 2007, respectively. He was with the GE Global Research Centre, Bengaluru, India, for one year in 2008. At GE, he contributed significantly to wireless power transfer, magneto-caloric refrigerator, perambulatory stroke detection, and subsea communication. In 2009, he joined as an Assistant Professor with the Department of Electrical Engineering, IIT Kanpur, where he has been a Full Professor, since November 2018. After joining IIT Kanpur, he has performed extensive research in the area of microwave engineering, such as microwave antennas, metamaterials, metamaterial absorbers and cloaking, FDTD technique, and MIMO Antennas. He has published more than 140 international journal articles and 170 conference papers in the last 16 years. He has two international patents also to his credit. He received various awards, such as the Cadence Gold Medal, in 2005, for Best M.Tech. Thesis at IIT Kanpur, the Institution of Engineers (IEI), India, Young Engineer Award, in 2014, the PK Kelkar Young Research Fellowship at IIT Kanpur, Letter of Appreciation from Director, IIT Kanpur, for outstanding teaching, and many awards for best papers in various conferences. He has been serving as the Sanjay and Rachna Pradhan Chair Professor, since April 2022. He is actively involved in a professional activity of the IEEE. He was a Secretary and a Treasurer of the IEEE UP Section (2012–2013) and 2015, respectively. He served as the Vice-Chair and the Chair of IEEE UP Section, in 2017 and 2018, respectively. He also served as an Executive Committee Member, IEEE India Council, from 2019 to 2020. He is the founding Chair of IEEE Antenna and Propagation Society Chapter, and Aerospace Electronics System Society Chapter, Uttar Pradesh Section, India.